Time-transformation approach to pulse propagation in nonlinear dispersive media: Inclusion of delayed Raman nonlinearity

Yuzhe Xiao,[1,*] Drew N. Maywar,[2] and Govind P. Agrawal[1]
[1]*The Institute of Optics, University of Rochester, Rochester, New York 14627, USA*
[2]*Electrical, Computer, and Telecommunications Engineering Technology, Rochester Institute of Technology, Rochester, New York 14623, USA*
(Received 12 February 2013; published 12 June 2013)

We extend our time-transformation technique to include the delayed Raman response and use it to study propagation of ultrashort, few-cycle, optical pulses inside a dispersive nonlinear medium. Our technique deals directly with the electric field associated with an optical pulse and can be applied to pulses of arbitrary widths, as it does not make use of the slowly varying envelope approximation. We apply it to optical pulses containing several optical cycles and launched such that they form a third-order optical soliton. We vary the number of optical cycles within the pulse from 1 to 10 and study how the features such as soliton fission, intrapulse Raman scattering, and dispersive-wave generation depend on pulse width and soliton order. We find that for a fixed soliton order, the Raman-induced frequency shift becomes smaller, while the fraction of energy transferred to the dispersive wave increases, as pulse width is reduced. In the special case of a single-cycle pulse, the most dominant effect is self-steepening and it leads to dramatically different features in both the shape and spectrum of output pulses.

DOI: 10.1103/PhysRevA.87.063816 PACS number(s): 42.81.Dp, 42.65.Re

I. INTRODUCTION

The propagation of optical pulses inside nonlinear dispersive media such as optical fibers has been studied extensively over the last 20 years [1]. Such studies are not only relevant for designing optical-fiber communication systems [2], but they also have led to an entirely new field of supercontinuum generation with diverse applications [3]. With the development of ultrafast laser technology, optical pulses as short as 10 fs have become available commercially. Even attosecond pulses have been generated in recent years [4] with applications in a variety of fields [5]. For example, ultrashort pulses serve as a useful tool to resolve the ultrafast dynamics and are widely used in the field of ultrafast science [6]. An important question is how ultrashort pulses containing a single or a few optical cycles evolve inside a nonlinear dispersive medium.

As the width of an optical pulse becomes comparable to an optical cycle, the use of the nonlinear Schrödinger equation (NLSE) becomes questionable because the slowly varying envelope approximation is likely to break down in this region [1]. For this reason, the finite-difference time-domain (FDTD) method that solves Maxwell's equations directly is often used for ultrashort pulses [7,8]. However, the FDTD approach is limited to relatively short propagation distances (typically <1 mm) because it requires a step size that is a small fraction of the optical wavelength. In our recent work [9–11], we proposed an approach that deals directly with the electric field in the time domain, but does not suffer from this limitation. In our approach, the propagation of an optical pulse is implemented through a time transformation of the electric field. Dispersive effects can also be included in our time-transformation model, and its predictions agree fully with those of the NLSE [10] and the FDTD methods [11].

In our previous work [9–11], we focused on a Kerr medium and assumed that it responds instantaneously to the electric field. The nonlinear response of a medium to light generally has two parts. The first part comes from the response of electrons occurring on a time scale of under 1 fs. The other part, known as intrapulse Raman scattering [1], results from the response of molecules that is delayed by about 60 fs in the case of silica fibers. When pulse width becomes shorter than 100 fs, this delayed nonlinear response cannot be ignored.

In this paper, we extend our time-transformation approach to include the delayed nonlinear Raman response and apply it to study propagation of few-cycle optical pulses (as short as 1 fs) inside a dispersive nonlinear medium such as a silica waveguide. In Sec. II, we discuss how to include the delayed Raman response in our approach. We apply it in Sec. III for studying propagation of a short pulse, containing more than 10 optical cycles and launched to form a third-order soliton inside a silica waveguide, and confirm that our theory correctly predicts the nonlinear phenomena such as soliton fission, Raman-induced frequency shift, and dispersive-wave generation. In Sec. IV, we vary the number of optical cycles in the range of 1 to 10 and study how such nonlinear phenomena depend on the pulse width. As expected, the Raman-induced frequency shift decreases as the pulse gets narrower. More interestingly, a larger fraction of input pulse energy is transferred to the blue side of the input spectrum in the form of a dispersive wave. The case of single-cycle pulses is discussed in more details in Sec. V, where we show that the effects of self-steepening become dominant for such ultrashort pulses.

II. TIME-TRANSFORMATION APPROACH

As we discussed in our earlier work, the solution of Maxwell's equations (in a linear medium in the form of a waveguide so that transverse variations are irrelevant)

*Corresponding author: yuzhe.xiao@rochester.edu

can be written in an integral form under some reasonable assumptions [12],

$$E_{\text{out}}(t) = \int_{-\infty}^{\infty} h(t,t')E_{\text{in}}(t')dt', \tag{1}$$

where E_{in} and E_{out} are the input and output electric fields associated with the pulse and $h(t,t')$ is the impulse response function of the dielectric medium. Somewhat surprisingly, this relation can be applied to a nonlinear dielectric medium using a nonlinear transformation in the time domain [9–11]. In this approach, we include the delay of each temporal slice of the electric field inside the nonlinear medium through a temporal mapping that we refer to as time transformation. In Refs. [9–11], we applied this concept to a medium exhibiting the Kerr-type instantaneous nonlinearity. The central issue in this paper is whether the time-transformation technique can be used when the medium's nonlinear response is not instantaneous and is delayed by a duration that may exceed the pulse width itself. It turns out that the time-transformation model remains valid even when the delayed nonlinear response is considered because the simple picture of mapping each input slice to a corresponding output slice continues to hold. The only difference is that the refractive index now depends on light intensity in a delayed fashion.

To be more specific, we assume the following functional form for the medium's nonlinear response [1]:

$$R(t) = (1 - f_R)\delta(t) + f_R h_R(t), \tag{2}$$

where the first term accounts for the electronic response (Kerr type) and $h_R(t)$ represents the delayed Raman response function of molecules with a fractional contribution f_R. If we relate the refractive index of the medium to $R(t)$ as

$$n(t) = n_0 + n_2 \int_{-\infty}^{t} R(t - t')I(t')dt', \tag{3}$$

where n_0 is the linear part of the refractive index, n_2 is the nonlinear coefficient, and $I(t)$ is the intensity, we obtain

$$n(t) = n_0 + n_2\left[(1 - f_R)I(t) + f_R \int_{-\infty}^{t} h_R(t - t')I(t')dt'\right]. \tag{4}$$

In the time-transformation approach, the transit time of a temporal slice located at t' is given by $t_1 = n(t')L/c$, where L is the medium length and c is the speed of light in vacuum. It follows from the form of Eq. (4) that the transit time consists of three parts and can be written as

$$t_1 = n(t')L/c = T_{\text{Linear}} + T_{\text{Kerr}} + T_{\text{Raman}}. \tag{5}$$

The first part of the transit time, $T_{\text{Linear}} = n_0 L/c$, comes from the linear part of the refractive index and provides the dominant contribution. The nonlinear part of the transit time has two contributions related to the instantaneous and delayed part of the nonlinearity. These are given by

$$T_{\text{Kerr}} = (n_2 L/c)(1 - f_R)I(t'), \tag{6}$$

and

$$T_{\text{Raman}} = n_2 f_R \frac{L}{c} \int_{-\infty}^{t'} h_R(t' - t'')I(t'')dt''. \tag{7}$$

Equation (5) represents the nonlinear transformation (or mapping) of the time t' of a temporal slice time to a new time t_1. We use this transformation in Eq. (1) and write this equation as

$$E_{\text{out}}(t) = \int_{-\infty}^{\infty} h(t - t_1)E'(t_1)J(t_1)dt_1, \tag{8}$$

where $E'(t_1) = E_{\text{in}}(t')$, and the Jacobian of the transformation is given by

$$J(t_1) = dt'/dt_1 = (1 + dT_{\text{Kerr}}/dt' + dT_{\text{Raman}}/dt')^{-1}. \tag{9}$$

The important point to note is that our time transformation allows us to write Eq. (8) in the form of a convolution. As a result, we can perform the integral numerically in the frequency domain using the convolution theorem, provided we know the functional form of the impulse response function $h(t)$. As we discussed in Ref. [10], the Fourier transform of $h(t)$ is given by

$$\tilde{h}(\omega) = \exp[i\beta(\omega)L], \tag{10}$$

where $\beta(\omega)$ is the propagation constant, defined as $\beta(\omega) = n_0(\omega)\omega/c$. Thus, the dispersion nature of the medium is contained fully in its impulse response function $h(t)$.

In the following numerical calculations, the dispersive effects are considered by expanding the propagation constant $\beta(\omega)$ in a Taylor series around the carrier frequency ω_0 of the pulse and retaining terms up to third order in $\omega - \omega_0$:

$$\beta(\omega) \approx \beta_0 + \beta_1(\omega - \omega_0) + \frac{\beta_2}{2}(\omega - \omega_0)^2 + \frac{\beta_3}{6}(\omega - \omega_0)^3, \tag{11}$$

where $\beta_0 = n_0(\omega_0)\omega_0/c$, and β_1, β_2, and β_3 are the first-, second-, and third-order dispersion parameters, respectively. For few-cycle pulses, it may be necessary to include other higher-order dispersion terms or even to use the Lorentz model to account for dispersion fully. In this work, we include dispersion only up to third order to emphasis the role of delayed Raman response. The inclusion of higher-order terms does not affect our conclusions.

Note that we made an implicit assumption in writing the expressions for T_{Kerr} and T_{Raman}, namely, that the pulse shape does not change considerably over the propagation length L. Since pulse shape generally does not change much over distances that are a small fraction of the dispersion length, Eq. (8) needs to be solved in a stepwise fashion by dividing the medium length into multiple sections, similar to the split-step Fourier method used for solving the NLSE [1].

III. COMPARISON WITH THE NLSE APPROACH

Before we consider single- or few-cycle pulses, we apply our approach to a relatively wide optical pulse containing more than 10 cycles and compare the results with those obtained using the generalized NLSE. More specifically, we consider the propagation of a third-order soliton and assume that the input electric field is given by

$$E_{\text{in}}(t) = \text{Re}[\sqrt{I_0}\,\text{sech}(t/T_0)e^{-i\omega_0 t}], \tag{12}$$

where we choose the carrier frequency $\omega_0/2\pi = 200$ THz, corresponding to an input wavelength of 1.5 μm. We set

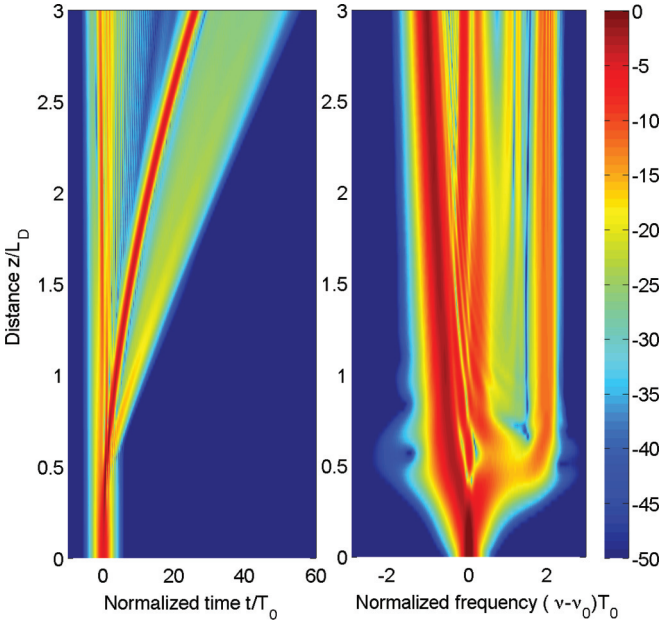

FIG. 1. (Color online) Evolution of temporal and spectral profiles over three dispersion lengths when an input pulse with $T_0 = 30$ fs forms a third-order soliton. The intensities are plotted using a normalized 50 dB color scale.

$T_0 = 30$ fs to ensure that the input pulse has more than 10 cycles and let it propagate in the anomalous-dispersion region ($\beta_2 < 0$) of a silica waveguide, where an optical soliton can form. The peak intensity I_0 of the pulse is chosen so that it corresponds to a third-order soliton [1]: $N = (\beta_0 n_2 I_0 L_D)^{1/2} = 3$, where $L_D = T_0^2/|\beta_2|$ is the dispersion length. Third-order dispersion is also included using $\delta_3 = \beta_3/(6T_0|\beta_2|) = 0.06$, a typical value for silica waveguides. The Raman effect is included using the functional form of the Raman response function in Ref. [13].

Figure 1 shows the evolutions of temporal and spectral intensities over three dispersion lengths using our time-transformation approach. We repeated the same calculation by solving the generalized NLSE and the results were identical in all respects. The fission of third-order soliton occurs near $z = 0.5L_D$ in both cases, and the original soliton splits into three parts. Most of the energy goes into a much narrower Raman soliton that travels slower than the original pulse as its spectrum shifts continuously toward the red side (the broad peak on the left side). Some energy is also shed in the form of a dispersive wave at a frequency on the blue side of the input pulse spectrum (vertical line on the right side). The location of the blue-shifted peak agrees with the phase-matching condition associated with the generation of a dispersive wave [1]. The important point to stress is that our approach reproduces all known features and agrees completely with the NLSE results. In the next section, we consider pulses as short as a single optical cycle and discuss how the evolution of such pulses depends on their temporal duration.

IV. PROPAGATION OF FEW-CYCLE PULSES

As seen in the preceding section, propagation of short optical pulses inside a dispersive nonlinear medium exhibits

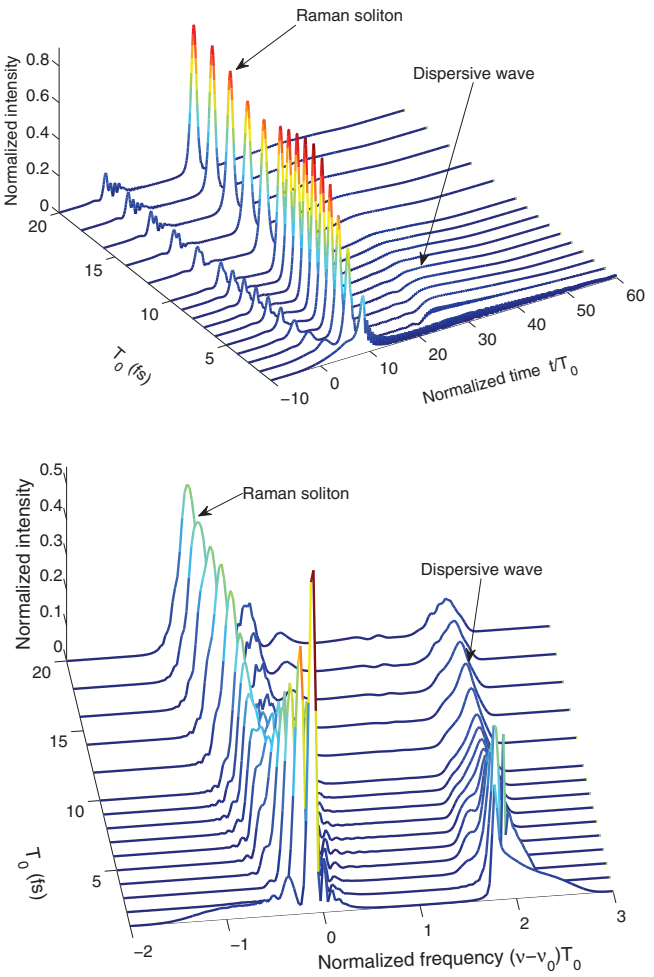

FIG. 2. (Color online) Comparison of pulse shapes and spectra at $z = 3L_D$ as T_0 is reduced from 20 to 1 fs. The input pulse corresponds to a third-order soliton in all cases.

rich dynamics through phenomena such as soliton fission, generation of dispersive wave, and four-wave mixing [14,15]. The question is what would happen if the pulse duration is reduced until the input pulse contains only a single optical cycle. To answer this question, we carried out a series of simulations by reducing T_0 in Eq. (12) from 20 fs (5 optical cycles) down to 1 fs (single cycle). We kept the same relative strengths of nonlinearity and dispersion so that a third-order soliton is formed in all cases. Figure 2 shows how the temporal shapes (top) and spectra (bottom) at a distance of $z = 3L_D$ change as pulses become shorter. As seen there, multiple changes occur, including a decrease in the Raman-induced frequency shift and an increase in energy of the dispersive wave, when T_0 is reduced from 20 to 2 fs. When T_0 is further decreased down to 1 fs, the output pulse exhibits even more drastic features. We discuss all such changes in what follows.

A. Intrapulse Raman scattering

As see in Fig. 2, for all pulse widths, a large fraction of input energy appears in a Raman soliton that travels slower than the input pulse because its spectrum has been shifted considerably toward the red side of the original spectrum. This change can

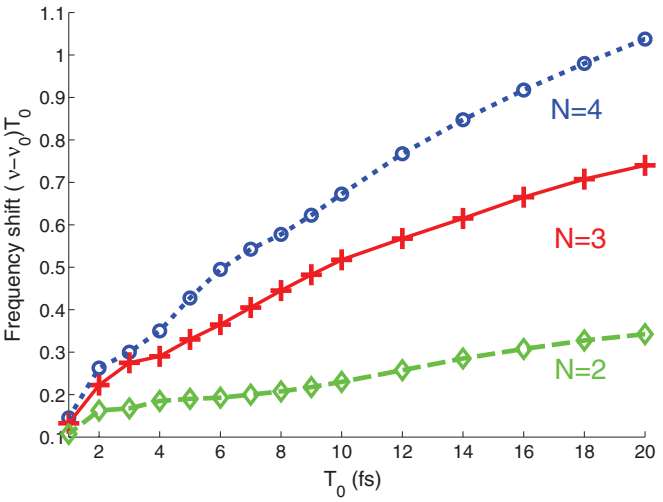

FIG. 3. (Color online) Changes in the Raman-induced frequency shift as T_0 is reduced from 20 to 1 fs for a fixed soliton order N. For the same value of T_0, pulses with a higher soliton order have larger frequency shifts.

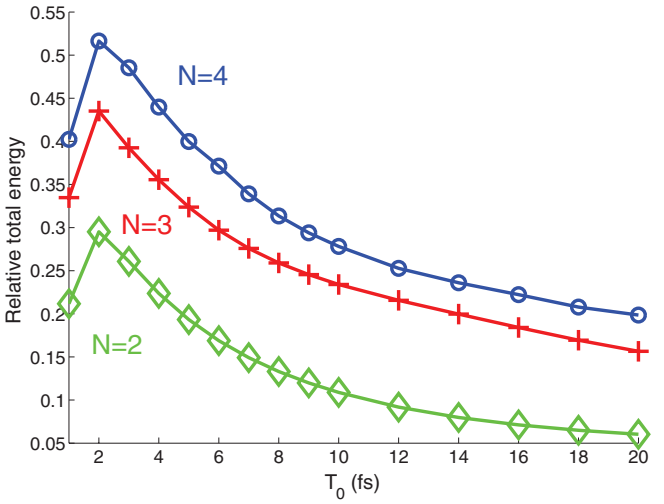

FIG. 4. (Color online) Energy of the dispersive wave as a function of T_0 for $N = 2$, 3, and 4. The drop for $T_0 < 2$ fs is related to the development of rapid temporal oscillations.

be expected since the Raman response time of about 60 fs for silica fibers is considerably larger than the pulse width. As the pulse becomes narrower, the influence of the delayed Raman response gets smaller. As a consequence, the Raman-induced frequency shift decreases for narrower pulses, which in return decreases the difference between the group velocities of the Raman soliton and rest of the pulse. The spectral shift of the Raman soliton decreases almost linearly until $T_0 = 10$ fs. When T_0 becomes smaller than this value, one cannot even see a clear spectral peak for the Raman soliton because it does not separate enough from the input spectrum.

To obtain the correct magnitude of the Raman-induced frequency shift as a function of pulse width T_0, we targeted the Raman soliton in the temporal domain, where a clear intensity peak is seen down to $T_0 = 1$ fs. By taking the Fourier transform of only this part of the pulse, we were able to deduce the spectral shift of the Raman soliton. Figure 3 shows the Raman-induced frequency shift as a function of T_0 for soliton orders of $N = 2$, 3, and 4. In these calculations, we increased the peak intensity of the input pulse to correspond to different soliton order, while keeping other parameters (n_2, β_2, and β_3) unchanged. It is expected that pulses with a larger N value would have a larger Raman-induced frequency shift because of their higher peak powers. As seen in Fig. 3, the amount of Raman-induced frequency shift decreases monotonically with decreasing T_0 for all three values of N. This is opposite to what is observed for pulses wider than the Raman response time of 60 fs, for which the Raman-induced frequency shift is known to scale as T_0^{-4} [1]. This qualitative difference between the short and long pulses is a manifestation of the fact that intrapulse Raman scattering is not an instantaneous nonlinear process and its response is delayed by about 60 fs in the case of silica glass.

B. Dispersive-wave generation

A significant feature of Fig. 2 is that as T_0 is reduced from 20 to 2 fs, more and more of the input pulse energy is transferred to a dispersive wave at a blue-shifted wavelength. This feature was also observed in Ref. [15], which focused on a pulse longer than 10 fs. Here we find that it persists for pulses as short as a single optical cycle. This feature is most clearly seen in the spectral domain in Fig. 2. To find the energy of this spectral peak, we integrated the spectral power density over the frequency range $1 < (\nu - \nu_0)T_0 < 3$ for different orders of solitons ($N = 2$, 3, and 4) with T_0 in the range of 1–20 fs. The results are shown in Fig. 4.

As see in Fig. 4, a higher-order soliton transfers more of its input energy into a dispersive wave. This feature agrees with the previous findings and is expected if we recall that a dispersive wave is generated by the perturbation of an optical soliton by the third-order dispersive effect. However, more interesting is the observation that for a given value of N, more energy can be transferred to a dispersive wave by reducing the input pulse width. One can see in Fig. 4 that more and more energy is transferred to the dispersive wave as T_0 decreases. However, the situation changes when T_0 is reduced to below 2 fs. Further investigation shows that this change is related to the impact of self-steepening. As the pulse width decreases, although the Raman response becomes weaker, the impact of the self-steepening effect governed by the parameter $s = (\omega_0 T_0)^{-1}$ becomes stronger. For example, the value of s is only 0.04 for 20 fs pulses, but it approaches 0.8 for $T_0 = 1$ fs at a carrier frequency of 200 THz. It turns out that when s exceeds 0.5, self-steepening leads to drastic changes in both the shape and the spectrum of optical pulses. Such changes are apparent in Fig. 2 when one compares the curves for $T_0 = 1$ and 2 fs. Since a pulse with $T_0 = 1$ fs contains only a single optical cycle, we focus on single-cycle pulses in the next section.

V. PROPAGATION OF SINGLE-CYCLE PULSES

As seen in Fig. 2, the temporal and spectral features change drastically when T_0 is reduced from 2 to 1 fs. In the temporal domain, the distinction between the original pulse, the Raman soliton, and the dispersive wave disappears, and we see a single dominant peak with a long tail exhibiting rapid oscillations.

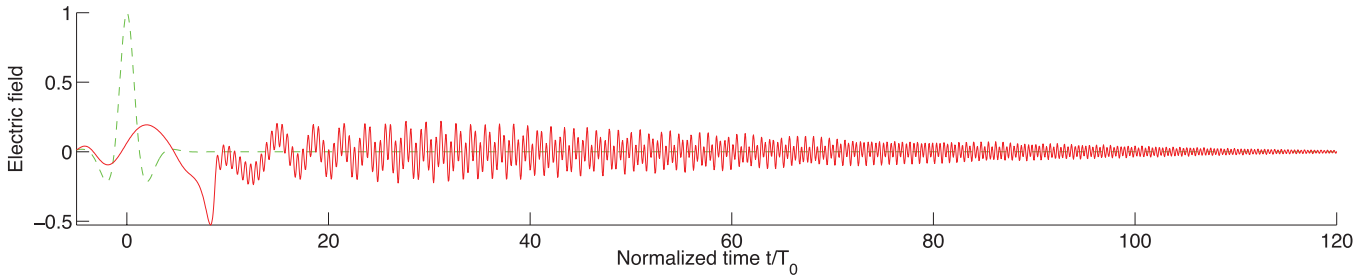

FIG. 5. (Color online) Electric field at a distance of $3L_D$ when a third-order soliton is excited using input pulse with $T_0 = 1$ fs. The input electric field is shown for comparison by dotted green curves.

The pulse spectrum becomes very asymmetric and develops many new frequency components both on the red side of the original carrier frequency peak and on the blue side of the dispersive-wave peak. In this section, we focus on these new features occurring when the input pulse contains a single optical cycle.

For single-cycle pulses, the concept of pulse envelope begins to lose its meaning. For this reason, we plot the actual electric field associated with the pulse. This is straightforward in our time-transformation approach since it deals directly with the electric field. Figure 5 shows the output electric field (solid red curve) at $z = 3L_D$ for a single-cycle input pulse, together with the input electric field (dotted green curve). As seen there, the electric field for $t < 5T_0$ appears to be a stretched version of the original electric field with reduced amplitude. However, for $t > 5T_0$, the behavior of the electric field becomes quite complicated and shows an oscillatory feature. These oscillations result from a beating between the frequency components near the input carrier frequency and those associated with the blue-shifted dispersive wave. They also occur for multicycle pulses, but their amplitude is negligibly small.

To understand this phenomenon more clearly, we show in Fig. 6 a spectrogram of the pulse exhibiting temporal and spectral features simultaneously. We employed a Gaussian-shaped sampling window function $W(t,\tau)$ to obtain spectral information for different temporal slices and calculated the spectrogram using

$$S(\omega,\tau) = \left| \int_{-\infty}^{\infty} W(t,\tau) E(t) e^{i\omega t} dt \right|^2 . \qquad (13)$$

We clearly see two spectral peaks, corresponding to spectral components around the carrier frequency and the frequency of the generated dispersive wave. Since these two peaks overlap in time, they interfere and produce temporal fringes in the time domain. A winglike structure is generated because the two spectral peaks fall on opposite sides of the zero-dispersion wavelength. This spectrogram explains the behavior of the electric field in Fig. 5. For example, for $t < 5T_0$, only one spectral peak occurs that is slightly red shifted because of intrapulse Raman scattering. After this point, multiple spectral components coexist together, and it is the beating among them that leads to distortion of the electric field and rapid oscillations in the pulse tail.

The spectrogram helps us in understanding the origin of rapid oscillations in the pulse temporal profile. However, one question still remains: what mechanism is responsible for the generation of such drastic changes in the electric field of single-cycle pulses? The answer turns out to be the self-steepening effect. As the pulse width is reduced, the relative strength of dispersion scales accordingly, since we employ the normalized versions of β_2 and β_3 in our study. The nonlinearity strength is also fixed because the soliton order N does not change. The only effect that is magnified for single-cycle pulses is the self-steepening effect. Indeed, the normalized parameter s takes a relatively large value of 0.8 for single-cycle pulses. To confirm that indeed self-steepening is behind the drastic changes, we repeated the simulation for single-cycle pulses by setting $s = 0$ so that self-steepening is absent, while keeping both the Kerr and Raman nonlinearity. The resulting pulse shape and spectrum are plotted by the dashed red curves in Fig. 7. For direct comparison, the solid blue curves show our results when everything is included and dotted green curves show the input pulse.

As seen in Fig. 7, when self-steepening is absent ($s = 0$), we see clearly three separate regions in the temporal domain that correspond to the residual input pulse near $t = 0$, a Raman soliton near $t = 10T_0$, and a dispersive wave near $t = 30T_0$. In the spectral domain, one can also clearly see

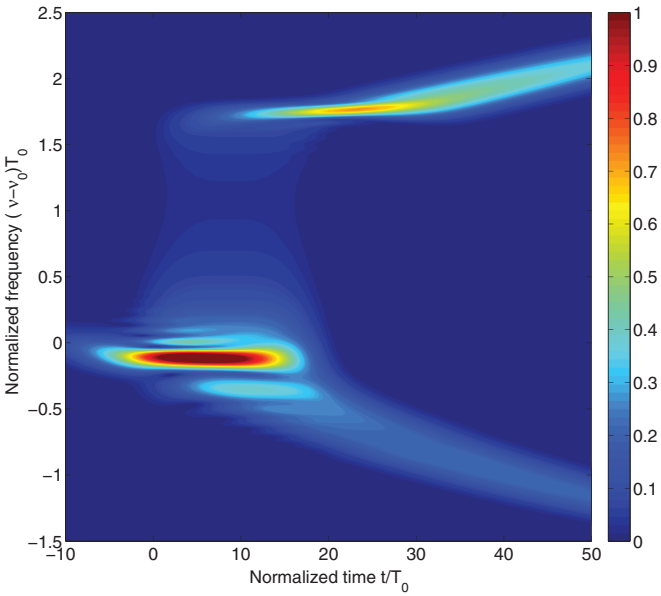

FIG. 6. (Color online) Spectrogram at $z = 3L_D$ for the $T_0 = 1$ fs case shown in Fig. 5. The intensity is plotted on a linear color scale.

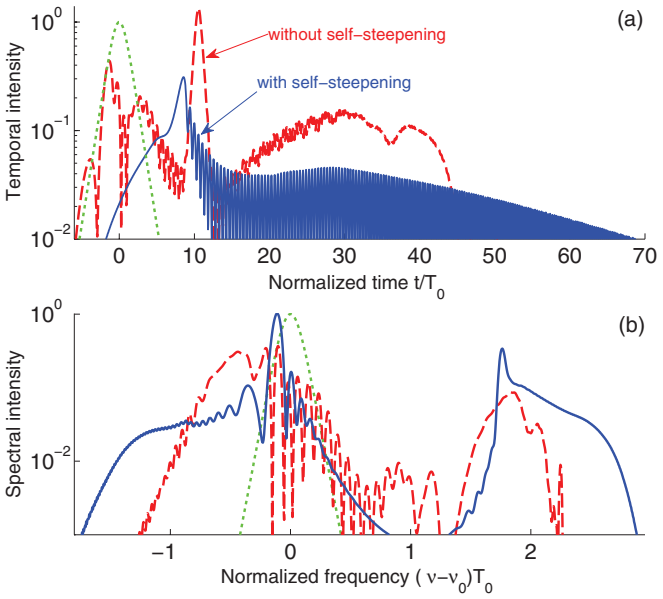

FIG. 7. (Color online) Impact of self-steepening on the (a) shape and (b) spectrum of a single-cycle input pulse. Self-steepening is turned off artificially for the dashed red curve, but is included fully for the solid blue curve. The input curves are shown by dotted green curves.

the corresponding spectral components. In particular, we see the red-shifted Raman soliton peak and a blue-shifted peak that corresponds to the dispersive wave. However, when self-steepening is present ($s = 0.8$), both the temporal and spectral intensity profiles change dramatically. In particular, in the time domain, the pulse exhibits a single dominant peak, together with an oscillatory tail that extends over a range exceeding $70T_0$. The peak amplitude is reduced considerably because a large fraction of the input pulse energy is now contained in the long oscillatory tail. This is also evident in the spectral domain, where the blue-shifted peak that corresponds to the dispersive wave is much broader with an asymmetric tail. We stress that third-order dispersion also plays an important role in generating the oscillating pulse tail. Indeed, oscillations disappear if we repeat this calculation with $\beta_3 = 0$.

VI. CONCLUDING REMARKS

In conclusion, we have extended our time-transformation technique to include the delayed Raman response and used it to study the propagation of ultrashort, few-cycle, optical pulses. Our technique deals directly with the electric field associated with an optical pulse and can be applied to pulses of arbitrary widths, as it does not make use of the slowly varying envelope approximation. We first apply this technique to a pulse containing more than 10 optical cycles and show that our approach reproduces the results obtained by solving the NLSE numerically. We then vary the width parameter T_0 from 1 to 20 fs and study how the features such as soliton fission, intrapulse Raman scattering, and dispersive-wave generation depend on pulse width and soliton order. We find that for a pulse with fixed soliton order, the Raman-induced frequency shift becomes smaller as pulse width decreases, while the fraction of energy transferred to the dispersive wave increases as pulse width is reduced. For the special case of a single-cycle pulse, the most dominant effect is self-steepening and leads to dramatically different features in both the pulse shape and pulse spectrum.

In this study, we applied the time-transformation method to pulses propagating inside optical waveguides, for which the spatial dependence of the waveguide mode does not change with propagation. Diffraction has to be considered in the case of bulk optical media. In this situation, one can apply the time-transformation method using the well-known angular spectrum approach [16].

ACKNOWLEDGMENT

This work is partially supported by the US Army Research Office.

[1] G. P. Agrawal, *Nonlinear Fiber Optics*, 5th ed. (Academic, New York, 2012).
[2] G. P. Agrawal, *Fiber-Optic Communication Systems*, 4th ed. (Wiley, New York, 2010).
[3] J. M. Dudley and J. R. Taylor, *Supercontinuum Generation in Optical Fibers* (Cambridge University Press, Cambridge, UK, 2010).
[4] G. Sansone, L. Poletto, and M. Nisoli, Nature Photon. **5**, 656 (2011).
[5] F. Krausz and M. Ivanov, Rev. Mod. Phys. **81**, 163 (2009).
[6] B. Kohler, V. V. Yakovlev, J. Che, J. L. Krause, M. Messina, K. R. Wilson, N. Schwentner, R. M. Whitnell, and Y. J. Yan, Phys. Rev. Lett. **74**, 3360 (1995).
[7] P. M. Goorjian and A. Taflove, Opt. Lett. **17**, 180 (1992).
[8] C. V. Hile and W. L. Kath, J. Opt. Soc. Am. B **13**, 1135 (1996).
[9] Y. Xiao, G. P. Agrawal, and D. N. Maywar, Opt. Lett. **37**, 1271 (2012).
[10] Y. Xiao, D. N. Maywar, and G. P. Agrawal, J. Opt. Soc. Am. B. **29**, 2958 (2012).
[11] Y. Xiao, D. N. Maywar, and G. P. Agrawal, Opt. Lett. **38**, 724 (2013).
[12] Y. Xiao, G. P. Agrawal, and D. N. Maywar, Opt. Lett. **36**, 505 (2011).
[13] Q. Lin and G. P. Agrawal, Opt. Lett. **31**, 3086 (2006).
[14] D. V. Skryabin and A. V. Yulin, Phys. Rev. E **72**, 016619 (2005).
[15] G. Chang, L.-J. Chen, and F. X. Krtner, Opt. Lett. **35**, 2361 (2010).
[16] J. W. Goodman, *Introduction to Fourier Optics*, 3rd ed. (Roberts, Greenwood Village, CO, 2004).